

Charge Transfer

Structure–Property Relationships in Click-Derived Donor–Triazole–Acceptor Materials

Paul Kautny,^{*[a]} Dorian Bader,^[a] Berthold Stöger,^[b] Georg A. Reider,^[c] Johannes Fröhlich,^[a] and Daniel Lumpi^[a]

Abstract: To shed light on intramolecular charge-transfer phenomena in 1,2,3-triazole-linked materials, a series of 1,2,3-triazole-linked push–pull chromophores were prepared and studied experimentally and computationally. Investigated modifications include variation of donor and/or acceptor strength and linker moiety as well as regioisomers. Photo-

physical characterization of intramolecular charge-transfer features revealed ambipolar behavior of the triazole linker, depending on the substitution position. Furthermore, non-centrosymmetric materials were subjected to second-harmonic generation measurements, which revealed the high nonlinear optical activity of this class of materials.

Introduction

Great efforts have been made in the design and synthesis of novel organic push–pull molecules owing to a wide range of technologically relevant applications. Bipolar organic materials, consisting of an electron-donating and -withdrawing subunit, are of crucial importance for organic light-emitting diodes (OLEDs),^[1] imaging,^[2] organic photovoltaics (OPVs),^[3] dyes, and nonlinear optical (NLO) materials^[4] for two-photon absorption^[5] or second-harmonic generation (SHG)^[6] to name a few. The electronic structure and, as a consequence, intrinsic properties of the individual molecules are dominated by the donor–acceptor interaction through intramolecular charge transfer (ICT).^[1a–c, 5a, 7]

Generally, the design of push–pull chromophores relies on a donor– π linker–acceptor architecture. Thus, the properties of the materials can be modified by careful selection of donor and/or acceptor units as well as by the modulation of the degree of electronic exchange between the donor and acceptor groups through the conjugated linker moiety.^[1a,b, 5a, 6a] To control ICT, molecular design offers a variety of specific linkage modes, such as 1) the introduction of sp^3 -hybridized bridges,^[8] 2) twisted configurations of molecules that result from sterically demanding groups,^[9] 3) *ortho* linkage of the electron-with-

drawing and -donating groups,^[10] and 4) *meta* linkage of the two molecular subunits to lower conjugation.^[10a,b, 11] Moreover, the choice of a specific linker moiety can be used effectively to control the donor–acceptor exchange. However, these particular methods are often difficult to realize and/or require tedious synthetic work.

In contrast, copper(I)-catalyzed azide–alkyne cycloaddition (CuAAC) is a well-investigated, robust synthetic methodology for joining two molecular subunits through 1,2,3-triazole formation. Whereas CuAAC, which is generally regarded as the most successful example of click chemistry,^[12] has been extensively exploited in many fields of organic synthesis,^[12, 13] reports on bipolar organic materials that incorporate 1,2,3-triazoles as functional π -conjugated moieties are rare. Such synthesized click-derived push–pull molecules have been employed as NLO materials,^[14] fluorophores,^[15] materials for two-photon absorption,^[16] fluorescent metal sensors,^[17] and electro-optical materials.^[18] CuAAC provides an intriguingly simple possibility to join various donor and acceptor combinations to establish the 1,2,3-triazole linker. However, the intrinsically weak electron-accepting properties of the triazole^[16, 18a, 19] and influence on ICT through the triazole linker have to be considered in the molecular design of the materials. Although a significant influence of the triazole substitution pattern on the electrochemical and photophysical properties has been reported,^[15b–e, 17e, 20] no extensive combinatorial study of a large set of donors and acceptors, including donor–acceptor exchange, can be found in the literature.

The aim of this work was to investigate the effects of donor and/or acceptor variations, as well as of triazole substitution pattern, on the photophysical properties of simple donor–triazole–acceptor molecules and gain a detailed insight into ICT phenomena to establish a structure–property relationship for this particular molecular scaffold.

[a] P. Kautny, D. Bader, Prof. Dr. J. Fröhlich, Dr. D. Lumpi
Institute of Applied Synthetic Chemistry, TU Wien
Getreidemarkt 9/163, 1060 Vienna (Austria)
E-mail: paul.kautny@tuwien.ac.at

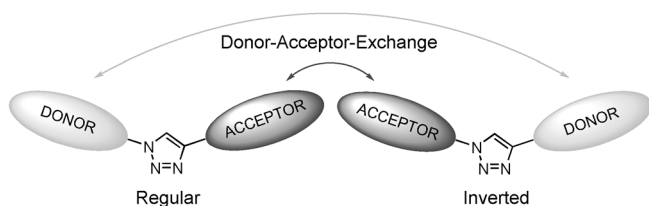
[b] Dr. B. Stöger
Institute of Chemical Technologies and Analytics, TU Wien
Getreidemarkt 9/164-SC, 1060 Vienna (Austria)

[c] Prof. Dr. G. A. Reider
Photonics Institute, TU Wien
Gußhausstraße 27–29, 1040 Vienna (Austria)

Supporting information and the ORCID number(s) for the author(s) of this article are available under <http://dx.doi.org/10.1002/chem.201603510>.

Results and Discussion

Our investigations are based on a large matrix of donor-acceptor molecules. We systematically increased donor (benzene < anisole < dimethylaniline (DMA)) and acceptor (benzene < pyridine < pyrimidine) strength to explore the ICT. Moreover, we examined the effects of donor-acceptor exchange, by inverting the triazole substitution pattern. In the following discussion, the two groups of regioisomers are referred to as the regular (electron donor at 1-N of the triazole linker) and inverted (electron donor at 4-C of the triazole linker) linked series (Scheme 1). An overview of all synthesized materials is given in Scheme 2.



Scheme 1. Representation of the investigated 1,2,3-triazole-linked donor-acceptor materials.

Synthesis

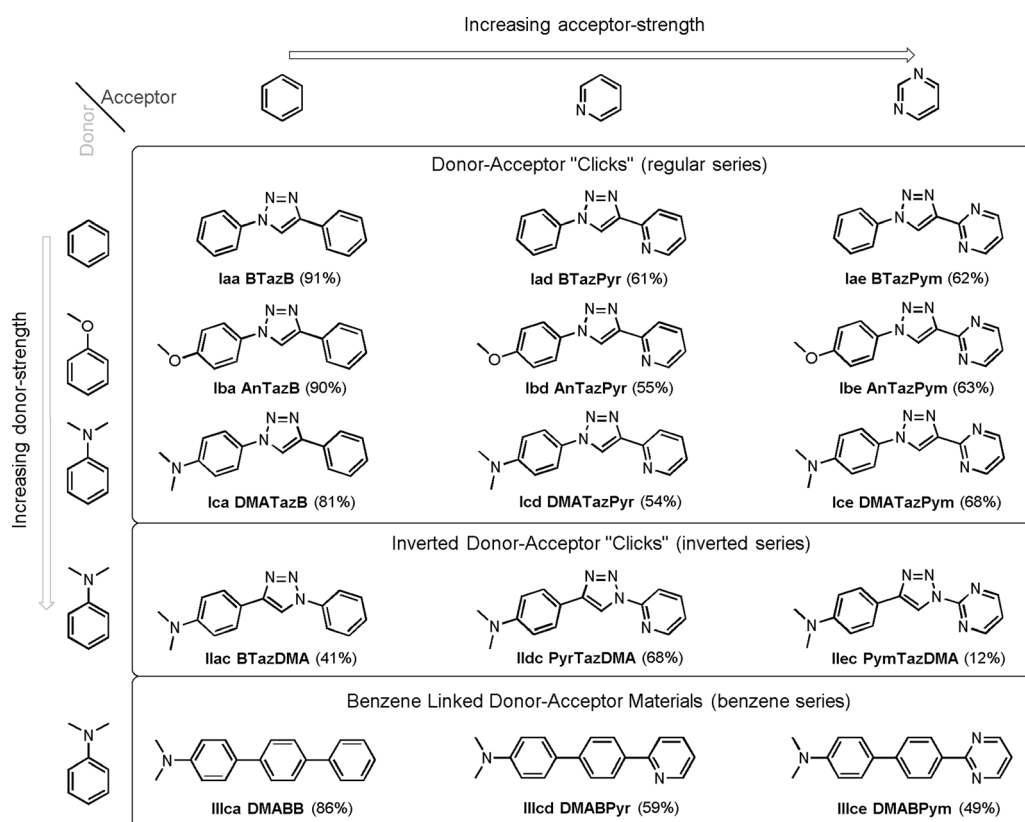
By employing standard CuAAC conditions, the synthesis of the regular series was accomplished by using $\text{CuSO}_4 \cdot 5\text{H}_2\text{O}$ as the

copper source and sodium ascorbate for the in situ reduction of Cu^{II} in a mixture of H_2O and $t\text{BuOH}$ (1:1; Scheme 3). Application of a reaction microwave (MW) reactor allowed for short reaction times (30–60 min). Whereas reactions starting from alkyne **2a** proceeded with excellent yields (81–91%), a tendency towards lower yields (54–68%) was observed in the conversion of electron-poor alkynes **2d** and **2e** (Scheme 3).

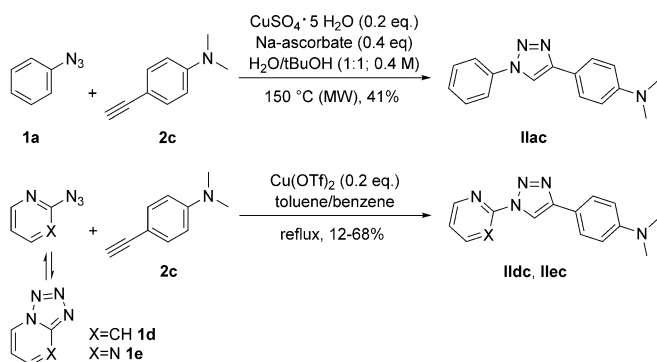


Scheme 3. Synthesis of the 1,2,3-triazole-linked donor-acceptor materials (regular series).

In case of the inverted series, DMA was employed as the sole donor, owing to its superior electron-donating properties (Scheme 4). The synthesis of pyridine- and pyrimidine-based **lldc** and **llce** required the application of 2-azidopyridine (**1d**) and 2-azidopyrimidine (**1e**). Whereas compound **llac** could be synthesized under standard click conditions (Scheme 4), this methodology was not applicable for azides **1d** and **1e** because they were in a tautomeric equilibrium with the corresponding ring-closed tetrazoles, and thus, exhibited significant-



Scheme 2. Overview of all materials under investigation.



Scheme 4. Synthesis of the 1,2,3-triazole-linked donor–acceptor materials (inverted series).

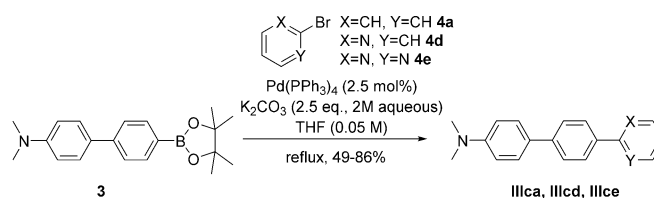
ly decreased reactivity. Single crystals of both tetrazoles were obtained from solutions of **2d** and **2e** in CDCl_3 upon slow evaporation of the solvent.

Nevertheless, by utilizing $\text{Cu}(\text{OTf})_2$ (OTf = triflate) as catalyst azides, compounds **1d** and **1e** could be reacted with **2c** by heating at reflux in toluene containing traces of benzene^[21] for 24–28 h to obtain **11dc** and **11ec** in 68 and 12% yield, respectively (Scheme 4).

Additionally, a benzene-linked donor–acceptor series was prepared to compare 1,2,3-triazole and benzene as linking moieties. DMA was likewise employed as the sole electron-donating group for this series and the strength of the electron acceptor was varied. Synthesis of the benzene-linked materials was realized in a Suzuki cross-coupling reaction starting from boronic ester **3** and the corresponding brominated acceptor moieties **4a**, **4d**, and **4e** (Scheme 5).

Photophysical characterization

To explore the effects of the systematic structural modifications on the photophysical properties of the materials, UV/Vis absorptions and emissions were recorded. In the following dis-



Scheme 5. Synthesis of the benzene-linked donor–acceptor materials.

cussion, all compounds are named according to the nomenclature defined in Scheme 2. All materials based on the DMA donor exhibited photoluminescence, with the exception of **PymTazDMA**, whereas among the other materials weak emission was only observed in the case of **AnTazPyr**. To examine the differences in the excited states of the compounds, photoluminescence spectra in eight solvents with increasing polarity (cyclohexane, dibutyl ether, diisopropyl ether, diethyl ether, dichloromethane, butanol, ethanol, acetonitrile) have been recorded. However, in butanol and ethanol, no or only very weak emission was obtained from triazole-linked materials that incorporated pyridine or pyrimidine units, probably owing to specific protic interactions between the solvent and chromophores.^[15c,22] Key photophysical properties are summarized in Table 1 and all spectra of the individual compounds are given in the Supporting Information.

First, compounds of the regular series were investigated. Within this series, materials with a DMA donor unit exhibit similar absorption spectra in dichloromethane with broad maxima between $\lambda = 302$ and 309 nm. In contrast, the absorption profiles of materials with weaker donors seem to be predominately determined by the acceptor unit connected to the triazole at the 4-position. Although **BTazB** and **AnTazB** feature structured absorptions with several shoulders between $\lambda = 260$ and 290 nm, compounds **BTazPyr** and **AnTazPyr** exhibit a single absorption maximum at $\lambda = 287$ nm, albeit with low intensity in the case of **BTazPyr**. Pyrimidine-based **BTazPym** and **AnTazPym** feature one broad absorption peak at $\lambda = 255$ and

Table 1. Key photophysical properties of the materials.

	$\lambda_{\text{abs}}^{[a]}$ [nm]	$\epsilon^{[a]}$ [$\text{M}^{-1} \text{cm}^{-1}$]	$\lambda_{\text{PL,max}}^{[a]}$ [nm]	$\Delta E_{\text{opt.}}^{[a]}$ [eV]	$k^{[b]}$ [cm^{-1}]
BTazB	250.5, 266 (sh), ^[c] 272 (sh), ^[c] 282 (sh), ^[c] 289 (sh) ^[c]	23 140	n.o. ^[d]	4.04	–
BTazPyr	286.5	4020	n.o. ^[d]	4.02	–
BTazPym	255	25 120	n.o. ^[d]	4.18	–
AnTazB	256, 267 (sh), ^[c] 273 (sh), ^[c] 282 (sh), ^[c] 289 (sh) ^[c]	25 600	n.o. ^[d]	3.98	–
AnTazPyr	287	27 180	392.5	3.92	6087
AnTazPym	263	24 380	n.o. ^[d]	3.99	–
DMATazB	286 (sh), ^[c] 302	20 940	396	3.57	12 729
DMATazPyr	306	23 920	413.5	3.53	22 048
DMATazPym	309	20 020	454	3.49	27 609
DMABB	325	34 320	419.5	3.37	13 028
DMABPyr	337	27 640	449	3.22	18 636
DMABPym	351	30 000	472	3.10	20 865
BTazDMA	270 (sh), ^[c] 302	28 480	438	3.47	23 228
PyrTazDMA	271 (sh), ^[c] 296, 305 (sh), ^[c] 345 (sh) ^[c]	27 660	470.5	3.31	26 593
PymTazDMA	268 (sh), ^[c] 287, 310 (sh), ^[c] 345 (sh) ^[c]	16 760	n.o. ^[d]	3.20	–

[a] Determined in dichloromethane (5 μM). [b] Slope of the linear correlation of the Stokes shift with the solvent orientation polarizability determined from the Lippert–Mataga plots. [c] Shoulder. [d] Not observed.

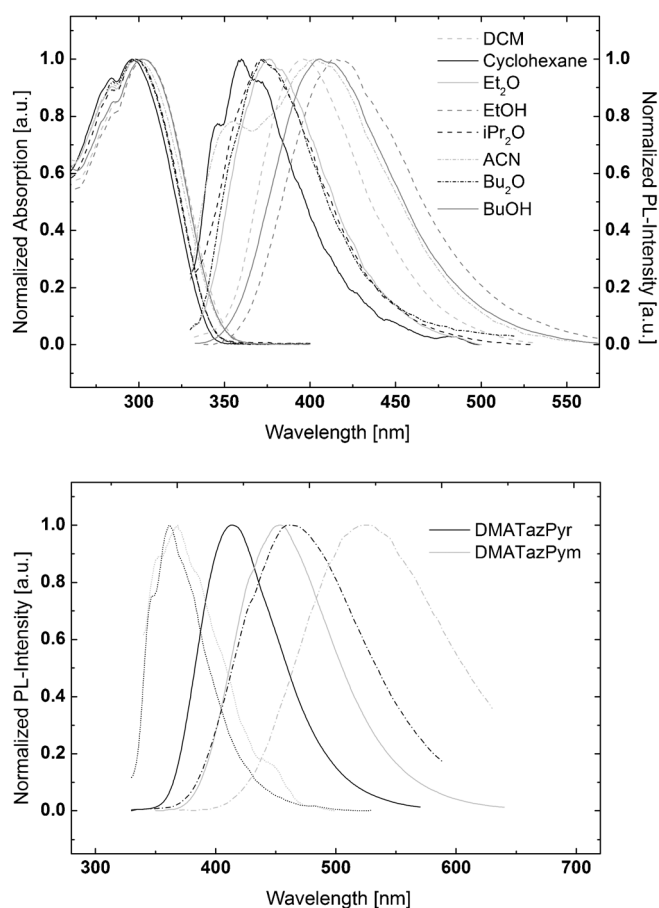


Figure 1. Top: UV/Vis absorption and photoluminescence emission spectra of **DMATazB** in various solvents (DCM = dichloromethane, ACN = acetonitrile). Bottom: photoluminescence emission spectra of **DMATazPyr** and **DMATazPym** in cyclohexane (.....), dichloromethane (—), and acetonitrile (---).

265 nm, respectively. Strikingly, the absorption onset, and thus, optical band gap of materials of the regular series is solely determined by the donor moiety and varies only insignificantly within the respective groups. Although materials with a benzene donor (**BTazB**, **BTazPyr**, **BTazPym**) exhibit optical band gaps between $\lambda = 297$ and 308 nm, onset values of the anisole derivatives are shifted to slightly higher wavelength ($\lambda = 311$ –316 nm). In contrast, the absorption onsets of compounds with DMA donors are distinctly redshifted and located between $\lambda = 347$ and 356 nm.

Whereas the absorption spectra are basically independent of the solvent polarity, the emission spectra of DMA-substituted materials of the regular series exhibit distinct solvatochromic effects, as typically observed for ICT emission.^[22] However, the extent of the solvatochromic shift strongly depends on the strength of the acceptor group (Figure 1). In cyclohexane, the emission maxima of **DMATazB**, **DMATazPyr**, and **DMATazPym** are vibronically resolved and located over a narrow range at $\lambda = 360$, 361.5, and 368.5 nm. In contrast, they are shifted to $\lambda = 396$, 413.5, and 454 nm in dichloromethane and $\lambda = 402.5$, 460.5, and 524.5 nm in acetonitrile, corresponding to an overall redshift of 42.5, 99, and 156 nm from cyclohexane to acetonitrile for **DMATazB**, **DMATazPyr**, and **DMATazPym**, respectively.

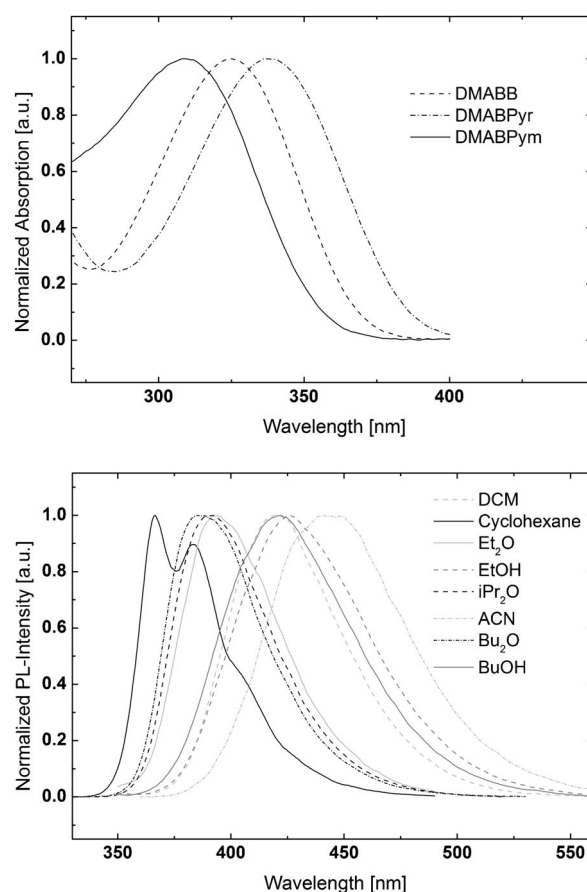


Figure 2. Top: UV/Vis absorption spectra of **DMABB**, **DMABPyr**, and **DMABPym** in dichloromethane. Bottom: photoluminescence emission spectra of **DMABB** in various solvents.

The increasingly redshifted emission can be attributed to the higher acceptor strength of pyridine and pyrimidine, and thus, an increased degree of charge transfer upon photoexcitation. Furthermore, an additional interesting emission feature was observed for **DMATazB**. In polar acetonitrile, a second high-energy emission band emerges at $\lambda = 354$ nm (Figure 1). Such dual behavior is indicative of a mixed emission from a locally excited (LE) and ICT state; a feature that has been previously reported for structurally related chromophores.^[15b]

As a second step, the benzene-linked compounds were analyzed to identify varied photophysical properties relative to the regular series and correlate these alterations to the modified linkage mode. In contrast to the regular series, the absorption maxima and absorption onsets of benzene-linked materials are not only dependent on the donor unit, but exhibit progressive bathochromic shifts for stronger acceptor units (Figure 2). Accordingly, the absorption maxima of **DMABB**, **DMABPyr**, and **DMABPym** in dichloromethane are located at $\lambda = 325$, 337, and 351 nm; thus spanning a significantly larger range (26 nm corresponding to 0.28 eV) than that of the regular series (7 nm, 0.09 eV). This particular behavior can be explained by a donor–acceptor interaction in the ground state that is absent or distinctly reduced in the regular series. Moreover, the absorption maximum of **DMABB**, which is the compound with the weak-

est electron-accepting moiety within the series, is redshifted by 23 nm relative to that of the corresponding compound **DMATazB**. The observation of an acceptor dependence and overall redshift of the absorption are indicative of a higher degree of conjugation in the benzene-linked donor–acceptor materials. Thus, the incorporation of the triazole moiety in the regular series effectively decreased the electronic conjugation of the molecules in the ground state.

In analogy to the regular triazole series, all benzene-linked materials exhibited distinct solvatochromism, as depicted for **DMABB** in Figure 2. To provide a better insight into the solvent dependency of the emission and for better comparability of the different series the solvatochromic behavior of the materials the Lippert–Mataga equation^[23] [Eq. (1)] was applied:

$$(\nu_a - \nu_f) = \frac{2(\mu_e - \mu_g)^2}{hca^3} \Delta f + \text{const.} \quad (1)$$

in which $(\nu_a - \nu_f)$ is the Stokes shift, h is the Planck constant, c is the speed of light, a is the solvent cavity (Onsager) radius, and μ_g and μ_e correspond to the ground- and excited-state dipole moments, respectively. The orientation polarizability, Δf , as a measure of solvent polarity is related to the refractive index by Equation (2):

$$\Delta f = \frac{\varepsilon - 1}{2\varepsilon + 1} - \frac{n^2 - 1}{2n^2 + 1} \quad (2)$$

in which ε is the dielectric constant and n is the refractive index of the solvent. Equation (1) predicts a linear dependence between the Stokes shift and solvent polarity, for which the slope depends on the square of the dipole moment difference of the ground and excited states, and thus, indicates the degree of charge transfer upon photoexcitation. Because the molecular weight and shape of the investigated molecules are similar, slopes of the Lippert–Mataga plots are a direct measure of charge transfer in the individual molecules.

As seen in Figure 3, all materials indeed display a linear correlation of the Stokes shift and solvent polarity and steeper slopes were observed for materials that incorporated stronger acceptor units due to increased charge transfer. However, a comparison of both series unveils more complex behavior. Compounds **DMATazB** and **DMABB** exhibit nearly identical slopes of 12729 and 13028 cm^{-1} ; these values indicate similar degrees of charge transfer upon excitation. In contrast, the corresponding congeners with stronger acceptor units display different emission properties. Within the regular series, the slope values are distinctly increased to 22048 and 27609 cm^{-1} for the pyridine and pyrimidine acceptors, respectively, which suggests significantly enhanced charge transfer in these derivatives. In contrast, and in analogy to the absorption maxima, the benzene series exhibits an overall redshifted emission from **DMABB** to **DMABPyr** to **DMABPym**, which is already evident in cyclohexane. Furthermore, the additional redshift of the emission of the individual acceptor-substituted molecules caused by $\Delta\mu_{eg}$ is smaller than that of the regular series, as deduced from the lower slope values of **DMABPyr** (18636 cm^{-1})

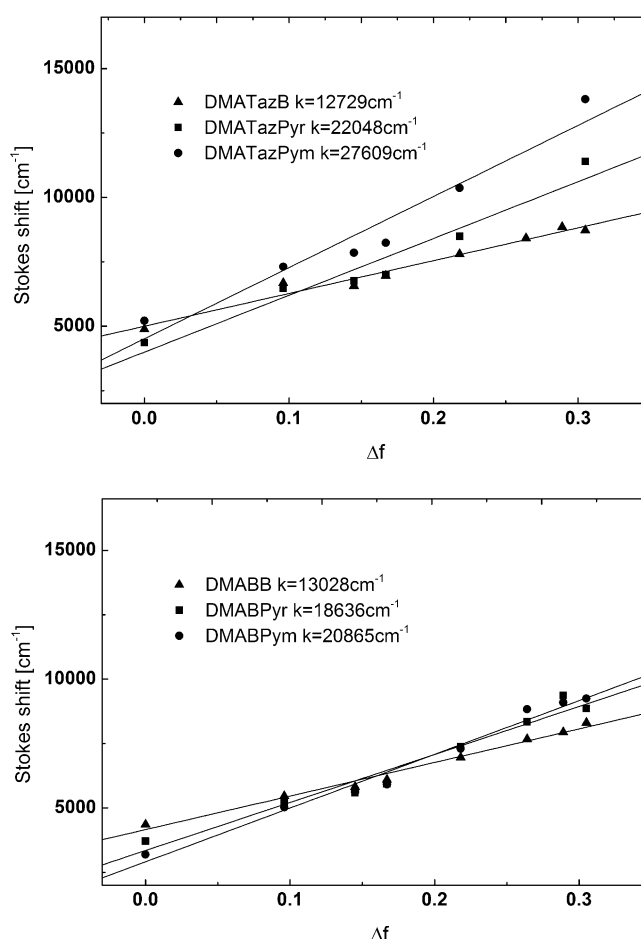
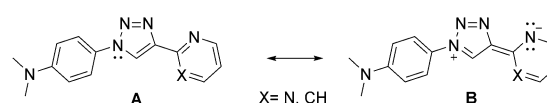


Figure 3. Lippert–Mataga plots of **DMATazB**, **DMATazPyr**, and **DMATazPym** (top), as well as of **DMABB**, **DMABPyr**, and **DMABPym** (bottom).

and **DMABPym** (20865 cm^{-1}); this indicates a lower degree of charge transfer.

From these findings, it can be concluded that the triazole linker decreases conjugation in the ground state, but enhances charge transfer upon photoexcitation. Notably, increased charge transfer is only observed in acceptor-substituted **DMATazPyr** and **DMATazPym**, whereas the charge-transfer properties of **DMATazB** are comparable to those of **DMABB**. Thus, it can be concluded that the triazole linker increases the donor strength of DMA, resulting in enhanced donor–acceptor interaction. The donor properties of the triazole linker can be rationalized by a contribution from mesomeric structure **B** (Scheme 6) to the excited state, as previously suggested for metallochromic materials.^[15e,17d]

Finally, the photophysical properties of the inverted series were determined. In contrast to the DMA-substituted deriva-



Scheme 6. Mesomeric structures of **DMATazPyr** and **DMATazPym**.

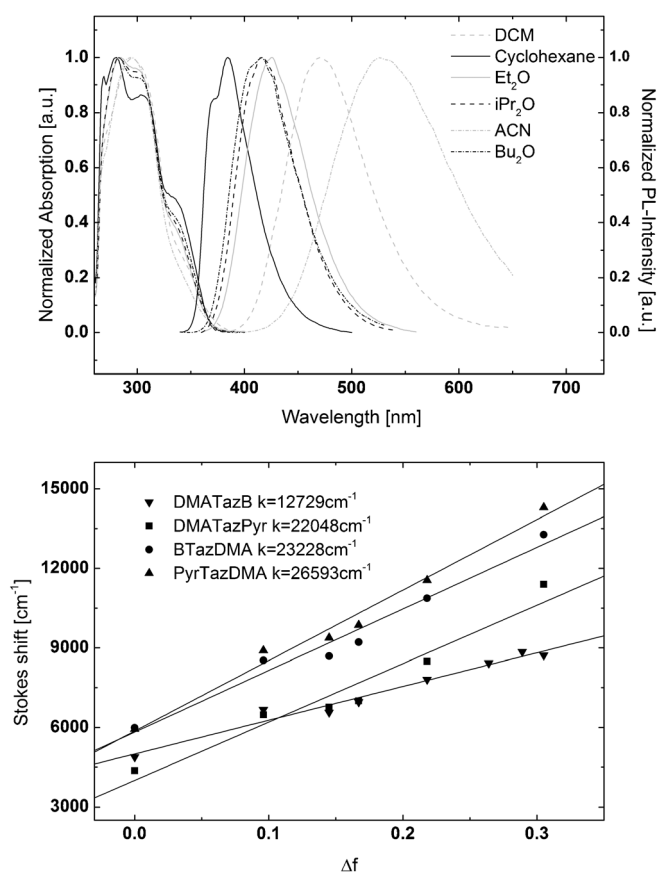


Figure 4. Top: UV/Vis absorption and photoluminescence emission spectra of **PyrTazDMA** in various solvents. Bottom: Lippert–Mataga plots of **DMA-TazB**, **DMATazPyr**, **BTazDMA**, and **PyrTazDMA**.

tives of the regular series, all materials of the inverted series display structured absorption spectra in solvents with low polarity, whereas the individual peaks diminish with increasing solvent polarity, as depicted for **PyrTazDMA** in Figure 4 as an example. In analogy to the benzene series, the absorption onsets of the inverted materials are gradually redshifted from **BTazDMA** to **PyrTazDMA** and **PymTazDMA**; this indicates a donor–acceptor interaction in the ground state that is not present in the regular series.

Whereas **BTazDMA** and **PyrTazDMA** exhibit strong solvatochromic behavior, no photoluminescent emission was detected for **PymTazDMA**. Emission maxima of **BTazDMA** and **PyrTazDMA** are redshifted relative to the corresponding derivatives of the regular series; a feature that has been previously reported for pairs of triazole regioisomers.^[15c] Strikingly, the value of the slope for **BTazDMA** ($23\,228\text{ cm}^{-1}$) is significantly higher than that of **DMATazB** ($12\,729\text{ cm}^{-1}$). The additional increase from **BTazDMA** to **PyrTazDMA** ($26\,593\text{ cm}^{-1}$) is due to the stronger electron-accepting moiety of the pyridine. However, it is distinctly lower than the corresponding two derivatives of the regular series. From the observation of a strong solvatochromic effect for **BTazDMA** without an additional acceptor unit, and the moderated increase of solvatochromism for the pyridine-substituted derivative **PyrTazDMA**, it can be concluded that the triazole itself operates as an electron-accepting moiety in the inverted series.

In summary, these investigations revealed that the triazole linkage significantly decreased conjugation in the ground state, but increased charge-transfer phenomena upon photoexcitation due to an enhancement of donor or acceptor properties. The kind of electronic interaction triggered by the ambipolar triazole moiety, in turn, can be controlled by the triazole substitution pattern.

Theoretical calculations

To gain further insight into the electronic properties of the investigated materials, theoretical studies applying DFT have been performed. The spatial distribution of the HOMOs and LUMOs of the compounds are depicted in Figure 5 and the Supporting Information.

HOMOs and LUMOs are uniformly distributed over the whole molecules in materials without strong acceptor and/or donor units. In contrast, increasing spatial separation can be found for materials with distinctive donor–acceptor combinations. This spatial separation of the HOMO and LUMO is indicative of a charge-transfer process upon photoexcitation, as described in the spectroscopic section. However, looking at the DMA-substituted congeners in detail, a more complex situation is observed (Figure 5). In **DMABPym**, the HOMO and LUMO are mainly located on the DMA and pyrimidine units, respectively,

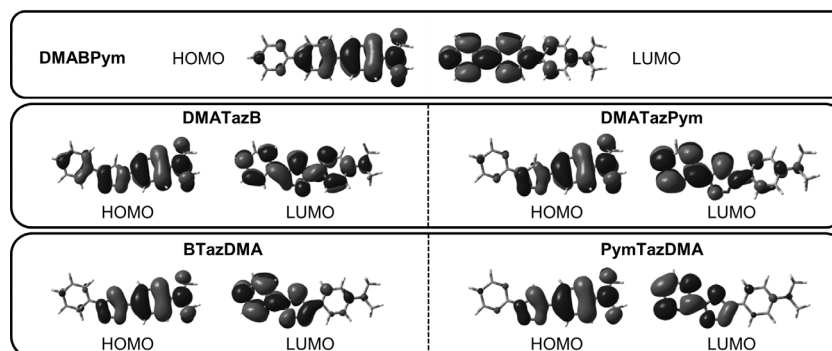


Figure 5. Spatial distribution of HOMO and LUMO levels of **DMABPym**, **DMATazB**, **DMATazPym**, **BTazDMA**, and **PymTazDMA**.

Table 2. Key crystallographic properties, supramolecular features, and relative SHG yields of the compounds under investigation.

	Space group	Centro-symmetry	Taz→Taz	Weak hydrogen bonds			π - π interactions		Relative SHG yield ^[a]
				Taz→Pym	Pym→Taz	Pym→Pym	Head-tail	Head-head	
BTazB ^[25]	<i>C2/c</i>	yes	chains						–
BTazPyr ^[26]	<i>P2₁/n</i>	yes	chains						–
BTazPym	<i>Cc</i>	no	chains				chains		80
AnTazB	<i>P2₁2₁2₁</i>	no	chains				chains		3.4
AnTazPyr	<i>P2₁2₁2₁</i>	no	chains				chains		6.0
AnTazPym	<i>P2₁/c</i>	yes		chains		chains			–
DMATazB ^[27]	<i>P2₁/n</i>	yes	chains						–
DMATazPyr ^[28]	<i>P2₁</i>	no					pairs		0.2
DMATazPym	<i>P2₁/c</i>	yes			pairs		pairs	chains ^[b]	–
BTazDMA ^[27]	<i>P1</i>	yes						pairs	–
PyrTazDMA	<i>P2₁/c</i>	yes					pairs	chains ^[b]	–
PymTazDMA	<i>P2₁/c</i>	yes			pairs		pairs	chains ^[b]	–

[a] Relative to potassium dihydrogen phosphate (KDP). [b] Formed by pairs of molecules.

but spread over the whole molecule and significant electron density is located on the opposite end of the molecule. A higher degree of separation is observed in **DMATazPym** and **PymTazDMA**, which indicates increased charge-transfer features; this is in agreement with experimental findings. In particular, the LUMO level of **PymTazDMA** is localized on the pyrimidine and triazole rings. This kind of localization was also found for the LUMO of **BTazDMA**. Likewise, the HOMO level of **BTazDMA** is confined to the DMA and triazole units. Thus, theoretical calculations suggest a pronounced charge transfer in **BTazDMA**, which is in agreement with spectroscopic characterization. In contrast, no such separation is observed in the corresponding derivative of the regular series, **DMATazB**. Therefore, this particular electronic layout can be directly attributed to the altered substitution of the triazole linker. A strong localization of the LUMO in **BTazDMA** in the absence of a strong electron-withdrawing unit indicates the establishment of an electron-accepting moiety at the benzene-triazole fragment. This particular behavior can be attributed to the substitution pattern of the triazole due to the absence of any other molecular modifications and is again in agreement with spectroscopic characterization.

Crystallography and NLO properties

Recently, our group reported a novel class of NLO-active materials with high SHG yields.^[14] These materials are based on click-functionalized ene-yne compounds with an 1,2,3-triazole linker as an essential building block. To further explore the scope of this class of materials, we investigated our present compounds with regard to their SHG efficiency. Because SHG requires non-centrosymmetric crystallization,^[24] single crystals of all triazole-linked materials were subjected to single-crystal XRD. Unfortunately, no usable crystals could be grown for the benzene-linked series. The crystal structures of **BTazB**,^[25] **BTazPyr**,^[26] **DMATazB**,^[27] **DMATazPyr**,^[28] and **BTazDMA**^[27] are known from the work of other groups. Additionally, we grew crystals and determined the structures of **AnTazB**, **AnTazPym**, **AnTazPyr**, **BTazPym**, **DMATazPym**, **PymTazDMA**, and **PyrTazDMA**. Moreover, we redetermined the structure of **DMATazB**, not

being aware of the previously published structural data.^[27] Key crystallographic properties of the materials are summarized in Table 2.

Compound **DMATazPyr** is made up of $Z' = 4$ crystallographically independent molecules. All other structures are made up of one independent molecule, located on a general position. Notably, common structural features were observed in some of the derivatives.

Compounds **AnTazB** and **AnTazPyr** are isostructural, which shows that pyridine can be used as a substitute for benzene. Likewise, compounds **DMATazPym**, **PymTazDMA**, and **PyrTazDMA** are isostructural, which shows that the substitution pattern of the triazole linker can be inverted and pyridine can be substituted by pyrimidine, without affecting the structure type. Whereas the inversion of the triazole has virtually no impact on the structure, additional hydrogen in the pyridine ring imposes a distinct stretching in the [100] direction (**DMATazPym**: $a = 8.4266(7)$ Å, **PymTazDMA**: $a = 8.5714(5)$ Å, **PyrTazDMA**: $a = 9.1392(8)$ Å). A more surprising structural relationship is observed for **BTazPyr** and **DMATazB**. Although the dimethylamine group in **DMATazB** requires additional space (**BTazPyr**: $V = 1078.45$ Å³, **DMATazB**: $V = 1315.84$ Å³), both structures can still be considered as isostructural (Figure S4.1 in the Supporting Information). The remaining structures (**BTazB**, **BTazPym**, **AnTazPym**, **DMATazPyr**, and **BTazDMA**) are unique.

Supramolecular features constitute, on one hand, weak hydrogen bonds of the triazole and pyrimidine hydrogen atoms, and, on the other hand, π - π interactions of the aromatic rings, as summarized in Table 2. The most commonly observed feature is hydrogen bonding connecting triazole moieties, forming infinite chains, for example, as in **BTazPyr** (Figure 6, left). Triazole to pyrimidine and pyrimidine to pyrimidine hydrogen bonds are only observed in **AnTazPym** (chains, Figure 6, right). Pyrimidine to triazole hydrogen bonds exist only in **DMATazPym** and **PymTazDMA** to form pairs of molecules. The absence of this particular intermolecular bonding in isostructural **PyrTazDMA** proves that these weak hydrogen bonds are not structure determining.

The π - π interactions are observed in **DMATazPyr** (pairs) and **DMATazPym**, **PymTazDMA**, and **PyrTazDMA**. In the last of

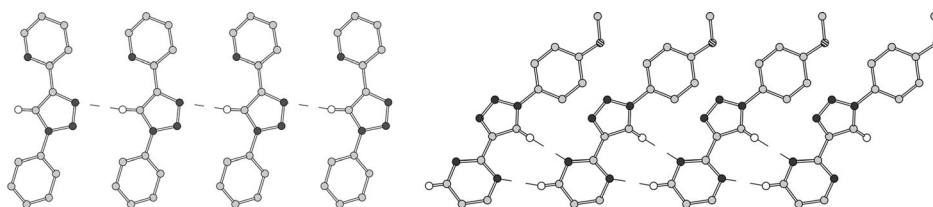


Figure 6. Supramolecular arrangement of **BTazPyr** (left) and **AnTazPym** (right) molecules in chains connected through Taz→Taz hydrogen bonds (**BTazPyr**) or Taz→Pym and Pym→Taz hydrogen bonds (**AnTazPyr**). Carbon, nitrogen, and oxygen atoms are represented by light gray, dark gray, and striped spheres of arbitrary radius. Hydrogen atoms not involved in hydrogen bonding are omitted for clarity. Hydrogen bonds are indicated by dashed lines.

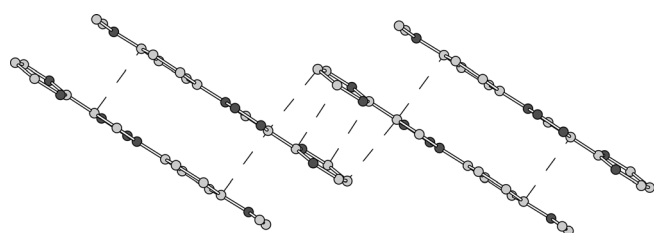


Figure 7. Supramolecular arrangement of **DMATazPym** determined by intermolecular π - π interactions. Colors are the same as those used in Figure 6. Intermolecular C-C contacts in the 3.3–3.4 Å range are indicated by dashed lines.

these, the resulting pairs are also connected by head-to-head π - π interactions (through pyrimidine/pyridine) to chains (Figure 7). Head-to-head π - π interactions through the benzene rings are also observed in **BTazDMA**; these form pairs of molecules. However, no intermolecular interaction between pairs is observed. Finally, the **BTazPym**, **AnTazB**, and **AnTazPyr** molecules are connected through head-to-tail π - π interactions to chains (Figure S4.2 in the Supporting Information).

All materials that crystallize as non-centrosymmetric crystals were investigated regarding their capability of SHG. The strong dependence of the macroscopic SHG yield on the exact alignment of the individual molecules with respect to the symmetry elements of the crystal has to be taken into account when different materials are compared.^[29] However, in the case of **AnTazB** and **AnTazPyr**, isostructural crystallization allows for the direct comparison of the two materials. Whereas **AnTazB** exhibits a SHG efficiency of 3.4 times the value of KDP, this value is higher for **AnTazPyr** (6.0×KDP). In analogy to DMA-substituted materials, stronger charge-transport features can be expected for **AnTazPyr** than those of **AnTazB**, owing to the presence of the pyridine acceptor. Thus, the increased SHG efficiency directly reflects the increased $\Delta\mu_{eg}$ value, as predicted by the two-state model.^[29] Investigation of the NLO properties of **BTazPym** revealed a significantly higher SHG yield of 80 times the value of KDP. We could therefore further improve the NLO performance compared with the most efficient click-functionalized thiophene- or selenophene-ring fragmentation^[14b] products reported previously by our group. Hence, our investigations further expand the scope of click-derived materials for NLO applications. In particular, the inverted triazole architecture, which ensures high $\Delta\mu_{egr}$, provides an appealing strategy in the design of new NLO materials because hyperpo-

larizability in the donor-acceptor materials is predominantly determined by ICT features.^[29]

Conclusion

We have synthesized a complete set of 1,2,3-triazole-linked donor-acceptor materials and provided a thorough photo-physical and theoretical characterization. Our findings reveal an intriguing relationship between intramolecular charge-transfer properties and triazole substitution patterns in donor-acceptor materials. Accordingly, triazole can be utilized not only as a linker unit, but also to increase either the electron-donating properties of the donor or to establish electron-accepting properties in a conjugated system without a defined acceptor moiety. Thus, our investigations provide guidelines for the incorporation of the 1,2,3-triazole unit as a linker in conjugated materials and are of great importance for the design of new functional click-derived materials for manifold applications.

Experimental Section

X-ray structure determination

Crystals of **BTazPym** (hexane/EtOH = 100:1), **AnTazB** (EtOH), **AnTazPyr** (hexane), **AnTazPym** (EtOH), **DMATazB** (EtOH), **DMATazPym** (EtOH), **PyrTazDMA** (EtOH), and **PymTazDMA** (EtOH) were crystallized from saturated boiling solvents. XRD intensities were collected at $T = 100$ K in a dry stream of nitrogen on Bruker Smart APEX (**AnTazPym** and **DMATazPym**) or Bruker Kappa APEX II (all other) diffractometer systems by using graphite-monochromatized $\text{Mo}_{K\alpha}$ radiation ($\lambda = 0.71073$ Å) and fine-sliced φ and ω scans. Data were reduced to intensity values with SAINT^[30] and an absorption correction was applied with the multiscan approach implemented in SADABS.^[30] The structures were solved by charge flipping by using SUPERFLIP^[31] and refined against F with JANA2006.^[32] Non-hydrogen atoms were refined anisotropically. The hydrogen atoms were placed in calculated positions and thereafter refined as riding on the parent atoms. Owing to a lack of anomalous scatterers, the Friedel opposites of non-centrosymmetric crystals were merged and the absolute structure was not determined. Molecular graphics were generated with the program MERCURY.^[33]

CCDC 1471390 (**AnTazB**), 1471391 (**AnTazPym**), 1471392 (**AnTazPyr**), 1471393 (**BTazPym**), 1471394 (**DMATazB**), 1471395 (**DMATazPym**), 1471396 (**PymTazDMA**), and 1471397 (**PyrTazDMA**) contain the supplementary crystallographic data for this paper. These data are provided free of charge by The Cambridge Crystallographic Data Centre.

SHG measurements

Second-order NLO properties of the substances were studied with second-harmonic measurements from powder samples. Powdered samples of the materials with a grain size of less than 1 μm were prepared with a mortar. A relative measurement of the NLO coefficients was possible with this technique because the second-harmonic efficiency scaled quadratically with the nonlinear coefficient, providing that the particle size was significantly less than the nonlinear coherence length (which was more than 10 μm in all practical cases).^[34] Subsequently, the powders were positioned between two microscope slides and irradiated with the output of an ultrafast Yb:KGW-Laser (Light Conversion, pulse duration 70 fs, average power 600 mW, repetition rate 75 MHz, wavelength $\lambda = 1034 \text{ nm}$), moderately focused with a 100 mm focusing lens. The diffusely reflected second-harmonic radiation was collected with a NA = 0.1 lens, separated from fundamental radiation with a color filter, and spectrally analyzed with a 0.25 m grating monochromator and a photomultiplier detector. The sample plane was positioned somewhat out of the focal plane (towards the lens) to prevent any damage to the sample. After each measurement, the samples were carefully checked for the absence of damage or thermal modification. For quantification of the SHG yields, (*Z*)-4-(2-(methylthio)-1-propenyl)-1-phenyl-1,2,3-triazole^[14a] was employed as a reference material (SHG yield of reference = SHG yield of KDP \times 2).

Synthesis

All reagents and solvents were purchased from commercial suppliers and used without further purification. Azidobenzene (**1a**),^[35] 1-azido-4-methoxybenzene (**1b**),^[36] 4-azido-*N,N*-dimethylbenzenamine (**1c**),^[36] **1d**,^[37] **1e**,^[37] 4-ethynyl-*N,N*-dimethylbenzenamine (**2c**),^[38] 2-ethynylpyridine (**2d**),^[38] 2-ethynylpyrimidine (**2e**),^[38] *N,N*-dimethyl-4'-(4,4,5,5-tetramethyl-1,3,2-dioxaborolan-2-yl)-[1,1'-biphenyl]-4-amine (**3**)^[39] were prepared in analogy to published procedures and the physical data of the prepared materials was compared with literature values. Anhydrous solvents were prepared by filtration through drying columns. Column chromatography was performed on silica 60 gel (Merck, 40–63 μm). Experiments under MW irradiation were performed in a Biotage Initiator Sixty MW reactor. Melting points were determined by using a MPA100 Opti-Melt automated melting point system from Stanford Research Systems. NMR spectra were recorded on a Bruker Avance DRX-400 spectrometer. A Thermo Scientific LTQ Orbitrap XL hybrid Fourier transform mass spectrometer equipped with a Thermo Fischer Exactive Plus Orbitrap (LC-ESI+) and a Shimadzu IT-TOF mass spectrometer were used for HRMS. UV/Vis absorption and fluorescence emission spectra in solution (5 μm) were recorded with a PerkinElmer Lambda 750 spectrometer and an Edinburgh FLS920 instrument, respectively. DFT calculations were performed by using the Gaussian 09 package.^[40] applying the Becke three-parameter hybrid functional with Lee–Yang–Perdew correlation (B3LYP)^[41] in combination with Pople basis sets 6-31G(d,p).^[42] Geometry optimizations were performed in the gas phase and without symmetry constraints. Orbital plots were generated by using GaussView.^[43]

General procedure for CuAAC

$\text{CuSO}_4 \cdot 5\text{H}_2\text{O}$ (0.2 equiv) and sodium ascorbate (0.4 equiv) were added to a solution of alkyne (1.0 equiv) and azide (1.0 equiv) in $\text{H}_2\text{O}/t\text{BuOH}$ (1:1; ca. 0.4 M) in a MW reaction vial immediately before the vial was sealed and the reaction mixture was heated to 150 °C until full conversion (TLC; 30–60 min). The resulting precipitate was dissolved in H_2O and DCM and the aqueous phase was

extracted with DCM. The combined organic layers were dried over Na_2SO_4 and concentrated under reduced pressure. Purification of the crude product was accomplished by filtration over a small amount of silica gel.

BTazB: Starting from ethynylbenzene (**2a**; 255 mg, 2.50 mmol, 1.00 equiv), **1a** (298 mg, 2.50 mmol, 1.00 equiv), $\text{CuSO}_4 \cdot 5\text{H}_2\text{O}$ (125 mg, 0.50 mmol, 0.2 equiv), and sodium ascorbate (198 mg, 1.00 mmol, 0.40 equiv), **BTazB** (506 mg, 91%) was obtained as a yellow solid. M.p. 181.0–182.3 °C; ^1H NMR (400 MHz, CD_2Cl_2): $\delta = 8.27$ (s, 1H), 7.92 (d, $J = 8.1 \text{ Hz}$, 2H), 7.81 (d, $J = 8.1 \text{ Hz}$, 2H), 7.58 (dd, $J = 8.0 \text{ Hz}$, 7.3 Hz, 2H), 7.51–7.45 (m, 3H) 7.37 ppm (t, $J = 7.3 \text{ Hz}$, 1H); ^{13}C NMR (100 MHz, CD_2Cl_2): $\delta = 148.7$, 137.7 131.0, 130.3, 129.5, 129.3, 128.9, 126.2, 121.0, 118.4 ppm; HRMS (ESI): m/z calcd for $\text{C}_{14}\text{H}_{11}\text{N}_3$: 221.09475 $[\text{M}]^+$, 222.10257 $[\text{M} + \text{H}]^+$, 244.08452 $[\text{M} + \text{Na}]^+$; found: 221.09438 $[\text{M}]^+$, 222.10196 $[\text{M} + \text{H}]^+$, 244.08379 $[\text{M} + \text{Na}]^+$.

AnTazB: Starting from **2a** (153 mg, 1.50 mmol, 1.00 equiv), **1b** (224 mg, 1.50 mmol, 1.00 equiv), $\text{CuSO}_4 \cdot 5\text{H}_2\text{O}$ (75 mg, 0.30 mmol, 0.2 equiv), and sodium ascorbate (119 mg, 0.60 mmol, 0.40 equiv), **AnTazB** (339 mg, 90%) was obtained as a white solid. M.p. 165.5–166.8 °C; ^1H NMR (400 MHz, CD_2Cl_2): $\delta = 8.17$ (s, 1H), 7.90 (d, $J = 8.2 \text{ Hz}$, 2H), 7.70 (d, $J = 9.0 \text{ Hz}$, 2H), 7.46 (dd, $J = 8.2 \text{ Hz}$, 7.4 Hz, 2H), 7.37 (t, $J = 7.4 \text{ Hz}$, 1H), 7.06 (d, $J = 9.0 \text{ Hz}$, 2H), 3.87 ppm (s, 3H); ^{13}C NMR (100 MHz, CD_2Cl_2): $\delta = 160.5$, 148.5, 131.2, 131.1, 129.5, 128.8, 126.2, 122.7, 118.6, 115.3, 56.2 ppm; HRMS (ESI): m/z calcd for $\text{C}_{15}\text{H}_{13}\text{N}_3\text{O}$: 251.10531 $[\text{M}]^+$, 252.11314 $[\text{M} + \text{H}]^+$, 274.09508 $[\text{M} + \text{Na}]^+$; found: 251.10486 $[\text{M}]^+$, 252.11195 $[\text{M} + \text{H}]^+$, 274.09465 $[\text{M} + \text{Na}]^+$.

DMATazB: Starting from **2a** (112 mg, 1.10 mmol, 1.00 equiv), **1c** (178 mg, 1.10 mmol, 1.00 equiv), $\text{CuSO}_4 \cdot 5\text{H}_2\text{O}$ (55 mg, 0.22 mmol, 0.20 equiv), and sodium ascorbate (87 mg, 0.44 mmol, 0.40 equiv), **DMATazB** (236 mg, 81%) was obtained as a yellow solid. M.p. 168.1–169.4 °C; ^1H NMR (400 MHz, CD_2Cl_2): $\delta = 8.13$ (s, 1H), 7.90 (d, $J = 8.1 \text{ Hz}$, 2H), 7.60 (d, $J = 9.0 \text{ Hz}$, 2H), 7.46 (dd, $J = 8.1 \text{ Hz}$, 7.4 Hz, 2H), 7.36 (t, $J = 7.4 \text{ Hz}$, 1H), 6.81 (d, $J = 9.0 \text{ Hz}$, 2H), 3.02 ppm (s, 6H); ^{13}C NMR (100 MHz, CD_2Cl_2): $\delta = 151.3$, 148.2, 131.4, 129.4, 128.6, 127.2, 126.2, 122.3, 118.4, 112.8, 40.8 ppm; HRMS (ESI): m/z calcd for $\text{C}_{16}\text{H}_{16}\text{N}_4$: 264.13695 $[\text{M}]^+$, 265.14477 $[\text{M} + \text{H}]^+$, 287.12672 $[\text{M} + \text{Na}]^+$; found: 264.13679 $[\text{M}]^+$, 265.14342 $[\text{M} + \text{H}]^+$, 287.12584 $[\text{M} + \text{Na}]^+$.

BTazPyr: Starting from **2d** (113 mg, 1.10 mmol, 1.00 equiv), **1a** (131 mg, 1.10 mmol, 1.00 equiv), $\text{CuSO}_4 \cdot 5\text{H}_2\text{O}$ (55 mg, 0.22 mmol, 0.20 equiv), and sodium ascorbate (87 mg, 0.44 mmol, 0.40 equiv), **BTazPyr** (148 mg, 61%) was obtained as a yellow solid. M.p. 90.7–92.0 °C; ^1H NMR (400 MHz, CD_2Cl_2): $\delta = 8.63$ (s, 1H), 8.60 (d, $J = 4.7 \text{ Hz}$, 1H), 8.21 (d, $J = 8.0 \text{ Hz}$, 1H), 7.85–7.80 (m, 3H), 7.57 (dd, $J = 8.3 \text{ Hz}$, 7.6 Hz, 2H), 7.48 (t, $J = 7.6 \text{ Hz}$, 1H), 7.27 ppm (dd, $J = 7.6$, 4.7 Hz, 1H); ^{13}C NMR (100 MHz, CD_2Cl_2): $\delta = 150.7$, 150.2, 149.6, 137.7, 137.4, 130.4, 129.4, 123.6, 121.0, 120.7, 120.6 ppm; HRMS (ESI): m/z calcd for $\text{C}_{13}\text{H}_{10}\text{N}_4$: 222.09000 $[\text{M}]^+$, 223.09782 $[\text{M} + \text{H}]^+$, 245.07977 $[\text{M} + \text{Na}]^+$; found: 222.08914 $[\text{M}]^+$, 223.09716 $[\text{M} + \text{H}]^+$, 245.07908 $[\text{M} + \text{Na}]^+$.

AnTazPyr: Starting from **2d** (105 mg, 1.02 mmol, 1.00 equiv), **1b** (152 mg, 1.02 mmol, 1.00 equiv), $\text{CuSO}_4 \cdot 5\text{H}_2\text{O}$ (51 mg, 0.20 mmol, 0.20 equiv), and sodium ascorbate (81 mg, 0.41 mmol, 0.40 equiv), **AnTazPyr** (141 mg, 55%) was obtained as an orange solid. M.p. 127.9–128.4 °C; ^1H NMR (400 MHz, CD_2Cl_2): $\delta = 8.59$ (d, $J = 4.7 \text{ Hz}$, 1H), 8.53 (s, 1H), 8.20 (d, $J = 8.1 \text{ Hz}$, 1H), 7.81 (dd, $J = 8.1$, 7.4 Hz,

1 H), 7.72 (d, $J=9.2$ Hz, 2H), 7.26 (d, $J=7.4$, 4.7 Hz, 1H), 7.06 (d, $J=9.2$ Hz, 2H), 3.87 ppm (s, 3H); ^{13}C NMR (100 MHz, CD_2Cl_2): $\delta=160.6$, 150.8, 150.1, 149.4, 137.4, 131.1, 123.5, 122.6, 120.8, 120.6, 115.4, 56.2 ppm; HRMS (ESI): m/z calcd for $\text{C}_{14}\text{H}_{12}\text{N}_4\text{O}$: 252.10056 $[\text{M}]^+$, 253.10839 $[\text{M}+\text{H}]^+$, 275.09033 $[\text{M}+\text{Na}]^+$; found: 252.10027 $[\text{M}]^+$, 253.10734 $[\text{M}+\text{H}]^+$, 275.08946 $[\text{M}+\text{Na}]^+$.

DMATazPyr: Starting from **2d** (88 mg, 0.85 mmol, 1.00 equiv), **1c** (138 mg, 0.85 mmol, 1.00 equiv), $\text{CuSO}_4 \cdot 5\text{H}_2\text{O}$ (42 mg, 0.17 mmol, 0.20 equiv), and sodium ascorbate (67 mg, 0.34 mmol, 0.40 equiv), **DMATazPyr** (121 mg, 54%) was obtained as a yellow solid. M.p. 150.7–151.5 °C; ^1H NMR (400 MHz, CD_2Cl_2): $\delta=8.59$ (d, $J=4.7$ Hz, 1H), 8.48 (s, 1H), 8.19 (d, $J=8.1$ Hz, 1H), 7.80 (dd, $J=8.1$, 7.4 Hz, 1H), 7.62 (d, $J=9.4$ Hz, 2H), 7.25 (d, $J=7.4$, 4.7 Hz, 1H), 6.81 (d, $J=9.2$ Hz, 2H), 3.02 ppm (s, 6H); ^{13}C NMR (100 MHz, CD_2Cl_2): $\delta=151.3$, 151.0, 150.1, 149.1, 137.3, 127.1, 123.3, 122.2, 120.6, 120.5, 112.8, 40.8 ppm; HRMS (ESI): m/z calcd for $\text{C}_{15}\text{H}_{15}\text{N}_5$: 265.13220 $[\text{M}]^+$, 266.14002 $[\text{M}+\text{H}]^+$, 288.12197 $[\text{M}+\text{Na}]^+$; found: 265.13254 $[\text{M}]^+$, 266.13866 $[\text{M}+\text{H}]^+$, 288.12122 $[\text{M}+\text{Na}]^+$.

BTazPym: Starting from **2e** (156 mg, 1.50 mmol, 1.00 equiv), **1a** (179 mg, 1.50 mmol, 1.00 equiv), $\text{CuSO}_4 \cdot 5\text{H}_2\text{O}$ (75 mg, 0.30 mmol, 0.20 equiv), and sodium ascorbate (119 mg, 0.60 mmol, 0.40 equiv), **BTazPym** (209 mg, 62%) was obtained as a yellow solid. M.p. 150.8–154.2 °C; ^1H NMR (400 MHz, CD_2Cl_2): $\delta=8.83$ (d, $J=4.9$ Hz, 2H), 8.74 (s, 1H), 7.84 (d, $J=8.9$ Hz, 2H), 7.58 (dd, $J=8.9$ Hz, 7.4 Hz, 2H), 7.50 (t, $J=7.4$ Hz, 1H), 7.27 ppm (t, $J=4.9$ Hz, 1H); ^{13}C NMR (100 MHz, CD_2Cl_2): $\delta=159.6$, 158.1, 148.6, 137.5, 130.4, 129.6, 123.7, 121.1, 120.4 ppm; HRMS (ESI): m/z calcd for $\text{C}_{12}\text{H}_9\text{N}_5$: 223.08525 $[\text{M}]^+$, 224.09307 $[\text{M}+\text{H}]^+$, 246.07502 $[\text{M}+\text{Na}]^+$; found: 223.08420 $[\text{M}]^+$, 224.09245 $[\text{M}+\text{H}]^+$, 246.07437 $[\text{M}+\text{Na}]^+$.

AnTazPym: Starting from **2e** (141 mg, 1.35 mmol, 1.00 equiv), **1b** (201 mg, 1.35 mmol, 1.00 equiv), $\text{CuSO}_4 \cdot 5\text{H}_2\text{O}$ (67 mg, 0.27 mmol, 0.20 equiv), and sodium ascorbate (107 mg, 0.54 mmol, 0.40 equiv), **AnTazPym** (216 mg, 63%) was obtained as a beige solid. M.p. 162.1–163.4 °C; ^1H NMR (400 MHz, CD_2Cl_2): $\delta=8.82$ (d, $J=4.8$ Hz, 2H), 8.65 (s, 1H), 7.73 (d, $J=9.1$ Hz, 2H), 7.25 (t, $J=4.8$ Hz, 1H), 7.07 (d, $J=9.1$ Hz, 2H), 3.87 ppm (s, 3H); ^{13}C NMR (100 MHz, CD_2Cl_2): $\delta=160.7$, 159.7, 158.1, 148.3, 130.8, 123.8, 122.7, 120.3, 115.4, 56.2 ppm; HRMS (ESI): m/z calcd for $\text{C}_{13}\text{H}_{11}\text{N}_5\text{O}$: 253.09581 $[\text{M}]^+$, 254.10364 $[\text{M}+\text{H}]^+$, 276.08558 $[\text{M}+\text{Na}]^+$; found: 253.09527 $[\text{M}]^+$, 254.10248 $[\text{M}+\text{H}]^+$, 276.08474 $[\text{M}+\text{Na}]^+$.

DMATazPym: Starting from **2e** (135 mg, 1.30 mmol, 1.00 equiv), **1c** (211 mg, 1.30 mmol, 1.00 equiv), $\text{CuSO}_4 \cdot 5\text{H}_2\text{O}$ (65 mg, 0.26 mmol, 0.20 equiv), and sodium ascorbate (103 mg, 0.52 mmol, 0.40 equiv), **DMATazPym** (234 mg, 68%) was obtained as a brown solid. M.p. 201.8–202.9 °C; ^1H NMR (400 MHz, CD_2Cl_2): $\delta=8.81$ (d, $J=4.9$ Hz, 2H), 8.60 (s, 1H), 7.63 (d, $J=9.2$ Hz, 2H), 7.24 (t, $J=4.9$ Hz, 1H), 6.81 (d, $J=9.2$ Hz, 2H), 3.02 ppm (s, 6H); ^{13}C NMR (100 MHz, CD_2Cl_2): $\delta=159.9$, 158.0, 151.4, 148.0, 126.9, 123.5, 122.3, 120.2, 112.7, 40.8 ppm; HRMS (ESI): m/z calcd for $\text{C}_{14}\text{H}_{14}\text{N}_6$: 266.12745 $[\text{M}]^+$, 267.13527 $[\text{M}+\text{H}]^+$, 289.11722 $[\text{M}+\text{Na}]^+$; found: 266.12824 $[\text{M}]^+$, 267.13384 $[\text{M}+\text{H}]^+$, 289.11640 $[\text{M}+\text{Na}]^+$.

BTazDMA: Starting from **2c** (232 mg, 1.60 mmol, 1.00 equiv), **1a** (192 mg, 1.60 mmol, 1.00 equiv), $\text{CuSO}_4 \cdot 5\text{H}_2\text{O}$ (80 mg, 0.32 mmol, 0.20 equiv), and sodium ascorbate (127 mg, 0.64 mmol, 0.40 equiv), **BTazDMA** (173 mg, 41%) was obtained as a yellow solid after column chromatography (petroleum ether (PE)/DCM, 1%). M.p. 175.0–176.6 °C; ^1H NMR (400 MHz, CD_2Cl_2): $\delta=8.11$ (s, 1H), 7.81–7.74 (m, 4H), 7.56 (dd, $J=8.6$ Hz, 7.4 Hz, 2H), 7.46 (t, $J=7.4$ Hz,

1H), 6.80 (d, $J=8.9$ Hz, 2H), 3.00 ppm (s, 6H); ^{13}C NMR (100 MHz, CD_2Cl_2): $\delta=151.3$, 149.3, 137.9, 130.3, 129.0, 127.2, 120.9, 118.8, 116.7, 112.9, 40.8 ppm; HRMS (ESI): m/z calcd for $\text{C}_{16}\text{H}_{16}\text{N}_4$: 264.13695 $[\text{M}]^+$, 265.14477 $[\text{M}+\text{H}]^+$, 287.12672 $[\text{M}+\text{Na}]^+$; found: 264.13640 $[\text{M}]^+$, 265.14382 $[\text{M}+\text{H}]^+$, 287.12537 $[\text{M}+\text{Na}]^+$.

PyrTazDMA

The synthesis of **PyrTazDMA** was accomplished according to a published procedure.^[21] Compounds **1d** (180 mg, 1.50 mmol, 1.00 equiv), **2c** (240 mg, 1.65 mmol, 1.10 equiv), and $\text{Cu}(\text{OTf})_2$ (108 mg, 0.30 mmol, 0.20 equiv) in toluene (6 mL, abs. degassed) and benzene (11 mg) were heated to reflux for 28 h. The reaction mixture was poured on H_2O and extracted with DCM. Subsequently, the combined organic layers were dried over Na_2SO_4 and concentrated under reduced pressure. The crude product was purified by column chromatography (DCM/ Et_2O , 2%) to yield **PyrTazDMA** (269 mg, 68%) as a yellow solid. M.p. 154.8–156.7 °C; ^1H NMR (400 MHz, CD_2Cl_2): $\delta=8.68$ (s, 1H), 8.52 (d, $J=4.7$ Hz, 1H), 8.20 (d, $J=8.2$ Hz, 1H), 7.94 (dd, $J=8.2$, 7.4 Hz, 1H), 7.79 (d, $J=9.0$ Hz, 2H), 7.36 (d, $J=7.4$, 4.7 Hz, 1H), 6.80 (d, $J=9.2$ Hz, 2H), 3.00 ppm (s, 6H); ^{13}C NMR (100 MHz, CD_2Cl_2): $\delta=151.3$, 150.0, 149.1, 148.9, 139.6, 127.2, 123.9, 118.8, 115.6, 114.1, 112.9, 40.8 ppm; HRMS (ESI): m/z calcd for $\text{C}_{15}\text{H}_{15}\text{N}_5$: 265.13220 $[\text{M}]^+$, 266.14002 $[\text{M}+\text{H}]^+$, 288.12197 $[\text{M}+\text{Na}]^+$; found: 265.13243 $[\text{M}]^+$, 266.13860 $[\text{M}+\text{H}]^+$, 288.12115 $[\text{M}+\text{Na}]^+$.

PymTazDMA

The synthesis of **PymTazDMA** was accomplished according to a published procedure.^[21] Compounds **1e** (157 mg, 1.30 mmol, 1.00 equiv), **2c** (208 mg, 1.43 mmol, 1.10 equiv), and $\text{Cu}(\text{OTf})_2$ (94 mg, 0.26 mmol, 0.20 equiv) in toluene (6 mL, abs. degassed) and benzene (3 drops) were heated to reflux for 24 h. The reaction mixture was poured on H_2O and extracted with DCM. Subsequently, the combined organic layers were dried over Na_2SO_4 and concentrated under reduced pressure. The crude product was purified by column chromatography (DCM/ Et_2O , 25%) to yield **PymTazDMA** (40 mg, 12%) as a yellow solid. M.p. 212 °C (dec); ^1H NMR (400 MHz, CD_2Cl_2): $\delta=8.87$ (d, $J=4.8$ Hz, 2H), 8.69 (s, 1H), 7.80 (d, $J=9.0$ Hz, 2H), 7.40 (t, $J=4.8$ Hz, 1H), 6.81 (d, $J=9.0$ Hz, 2H), 3.01 ppm (s, 6H); ^{13}C NMR (100 MHz, CD_2Cl_2): $\delta=159.8$, 155.2, 151.4, 148.9, 127.3, 121.1, 118.3, 117.1, 112.9, 40.7 ppm; HRMS (ESI): m/z calcd for $\text{C}_{14}\text{H}_{14}\text{N}_6$: 266.12745 $[\text{M}]^+$, 267.13527 $[\text{M}+\text{H}]^+$, 289.11722 $[\text{M}+\text{Na}]^+$; found: 266.12788 $[\text{M}]^+$, 267.13403 $[\text{M}+\text{H}]^+$, 289.11658 $[\text{M}+\text{Na}]^+$.

General procedure for the Suzuki cross-coupling reactions

Arylbromide (1.00 equiv), **3** (1.00 equiv), K_2CO_3 (2.50 equiv, 2 M degassed aqueous solution), and $[\text{Pd}(\text{PPh}_3)_4]$ (2.5 mol%) were added to degassed THF (50 mm). The mixture was heated to reflux under an argon atmosphere until full conversion (TLC, ca. 20 h). Subsequently, the solvent was evaporated and the residue was dissolved in DCM and H_2O . The aqueous phase was repeatedly extracted with DCM, the combined organic layers were dried over anhydrous Na_2SO_4 , and the solvent was removed in vacuo after filtration.

DMABB: Starting from bromobenzene (**4a**; 196 mg, 1.25 mmol, 1.00 equiv), **3** (404 mg, 1.25 mmol, 1.00 equiv), K_2CO_3 (432 mg, 3.13 mmol, 2.50 equiv, 2 M aqueous solution), and $[\text{Pd}(\text{PPh}_3)_4]$ (36 mg, 31 μmol , 2.5 mol%), **DMABB** (293 mg, 86%) was obtained as a yellow solid after column chromatography (PE/DCM, 40%). M.p. 239.8–241.7 °C; ^1H NMR (400 MHz, CD_2Cl_2): $\delta=7.67$ –7.65 (m,

6H), 7.56 (d, $J=9.0$ Hz, 2H), 7.46 (dd, $J=8.1$ Hz, 7.3 Hz, 2H), 7.35 (t, $J=7.3$ Hz, 1H), 6.82 (d, $J=9.0$ Hz, 2H), 3.00 ppm (s, 6H); ^{13}C NMR (100 MHz, CD_2Cl_2): $\delta=151.8, 141.4, 140.6, 139.1, 129.3, 128.6, 127.9, 127.8, 127.7, 127.3, 126.9, 113.2, 40.9$ ppm; HRMS (ESI): m/z calcd for $\text{C}_{20}\text{H}_{19}\text{N}$: 273.15120 $[M]^+$, 274.15903 $[M+H]^+$; found: 273.15102 $[M]^+$, 274.15784 $[M+H]^+$.

DMABPyr: Starting from 2-bromopyridine (**4d**; 198 mg, 1.25 mmol, 1.00 equiv), **3** (404 mg, 1.25 mmol, 1.00 equiv), K_2CO_3 (432 mg, 3.13 mmol, 2.50 equiv, 2 M aqueous solution), and $[\text{Pd}(\text{PPh}_3)_4]$ (36 mg, 31 μmol , 2.5 mol%), **DMABPyr** (204 mg, 59%) was obtained as a yellow solid after column chromatography (PE/DCM, 65%). M.p. 210.3–212.6 °C; ^1H NMR (400 MHz, CD_2Cl_2): $\delta=8.67$ (d, $J=4.8$ Hz, 1H), 8.06 (d, $J=8.6$ Hz, 2H), 7.81–7.74 (m, 2H), 7.68 (d, $J=8.6$ Hz, 2H), 7.59 (d, $J=9.0$ Hz, 2H), 7.22 (dd, $J=7.1, 4.8$ Hz, 1H), 6.82 (d, $J=9.0$ Hz, 2H), 3.00 ppm (s, 6H); ^{13}C NMR (100 MHz, CD_2Cl_2): $\delta=157.5, 150.9, 150.2, 142.1, 137.4, 137.2, 128.4, 128.0, 127.6, 126.7, 122.4, 120.5, 113.2, 40.8$ ppm; HRMS (ESI): m/z calcd for $\text{C}_{19}\text{H}_{18}\text{N}_2$: 275.15428 $[M+H]^+$; found: 275.15378 $[M+H]^+$.

DMABPym: Starting from 2-bromopyrimidine (**4e**; 199 mg, 1.25 mmol, 1.00 equiv), **3** (404 mg, 1.25 mmol, 1.00 equiv), K_2CO_3 (432 mg, 3.13 mmol, 2.50 equiv, 2 M aqueous solution), and $[\text{Pd}(\text{PPh}_3)_4]$ (36 mg, 31 μmol , 2.5 mol%), **DMABPym** (168 mg, 49%) was obtained as a yellow solid after column chromatography (DCM/ Et_2O , 1%). M.p. 198.8–201.1 °C; ^1H NMR (400 MHz, CD_2Cl_2): $\delta=8.79$ (d, $J=4.8$ Hz, 2H), 8.47 (d, $J=8.6$ Hz, 2H), 7.70 (d, $J=8.6$ Hz, 2H), 7.61 (d, $J=9.0$ Hz, 2H), 7.18 (t, $J=4.8$ Hz, 1H), 6.82 (d, $J=9.0$ Hz, 2H), 3.01 ppm (s, 6H); ^{13}C NMR (100 MHz, CD_2Cl_2): $\delta=165.0, 157.8, 151.0, 143.8, 135.8, 129.0, 128.3, 128.1, 126.4, 119.4, 113.1, 40.8$ ppm; HRMS (ESI): m/z calcd for $\text{C}_{18}\text{H}_{17}\text{N}_3$: 275.14170 $[M]^+$, 276.14952 $[M+H]^+$; found: 275.14163 $[M]^+$, 276.14840 $[M+H]^+$.

Acknowledgements

This work was supported in part by the TU Wien research funds. The X-ray center of the TU Wien is acknowledged for providing access to the single-crystal diffractometer.

Keywords: charge transfer • chromophores • donor–acceptor systems • nonlinear optics • triazoles

- [1] a) Y. Tao, C. Yang, J. Qin, *Chem. Soc. Rev.* **2011**, *40*, 2943–2970; b) A. Chaskar, H.-F. Chen, K.-T. Wong, *Adv. Mater.* **2011**, *23*, 3876–3895; c) Y. Tao, K. Yuan, T. Chen, P. Xu, H. H. Li, R. F. Chen, C. Zheng, L. Zhang, W. Huang, *Adv. Mater.* **2014**, *26*, 7931–7958; d) M. Zhu, C. Yang, *Chem. Soc. Rev.* **2013**, *42*, 4963–4976; e) W.-C. Chen, C.-S. Lee, Q.-X. Tong, *J. Mater. Chem. C* **2015**, *3*, 10957–10963.
- [2] a) X. Qian, Y. Xiao, Y. Xu, X. Guo, J. Qian, W. Zhu, *Chem. Commun.* **2010**, *46*, 6418–6436; b) S. J. Lord, N. R. Conley, H.-I. D. Lee, S. Y. Nishimura, A. K. Pomerantz, K. A. Willets, Z. Lu, H. Wang, N. Liu, R. Samuel, R. Weber, A. Semyonov, M. He, R. J. Twieg, W. E. Moerner, *ChemPhysChem* **2009**, *10*, 55–65.
- [3] a) A. Mishra, P. Bäuerle, *Angew. Chem. Int. Ed.* **2012**, *51*, 2020–2067; *Angew. Chem.* **2012**, *124*, 2060–2109; b) J. Roncali, *Acc. Chem. Res.* **2009**, *42*, 1719–1730; c) Y.-J. Cheng, S.-H. Yang, C.-S. Hsu, *Chem. Rev.* **2009**, *109*, 5868–5923; d) H. Zhou, L. Yang, W. You, *Macromolecules* **2012**, *45*, 607–632.
- [4] a) M. J. Cho, D. H. Choi, P. A. Sullivan, A. J. P. Akelaitis, L. R. Dalton, *Prog. Polym. Sci.* **2008**, *33*, 1013–1058; b) S.-i. Kato, F. Diederich, *Chem. Commun.* **2010**, *46*, 1994–2006; c) L. R. Dalton, *Pure Appl. Chem.* **2004**, *76*, 1421–1433; d) S. R. Marder, *Chem. Commun.* **2006**, 131–134.
- [5] a) G. S. He, L.-S. Tan, Q. Zheng, P. N. Prasad, *Chem. Rev.* **2008**, *108*, 1245–1330; b) M. Pawlicki, H. A. Collins, R. G. Denning, H. L. Anderson, *Angew. Chem. Int. Ed.* **2009**, *48*, 3244–3266; *Angew. Chem.* **2009**, *121*, 3292–3316; c) H. Myung Kim, B. Rae Cho, *Chem. Commun.* **2009**, 153–164.
- [6] a) L. R. Dalton, P. A. Sullivan, D. H. Bale, *Chem. Rev.* **2009**, *109*, 25–55; b) T. Verbiest, S. Houbrechts, M. Kauranen, K. Clays, A. Persoons, *J. Mater. Chem.* **1997**, *7*, 2175–2189; c) J. A. Delaire, K. Nakatani, *Chem. Rev.* **2000**, *100*, 1817–1846.
- [7] Y. Shirota, H. Kageyama, *Chem. Rev.* **2007**, *107*, 953–1010.
- [8] a) M. Guan, Z. Q. Chen, Z. Q. Bian, Z. W. Liu, Z. L. Gong, W. Baik, H. J. Lee, C. H. Huang, *Org. Electron.* **2006**, *7*, 330–336; b) L. C. Zeng, T. Y. H. Lee, P. B. Merkel, S. H. Chen, *J. Mater. Chem.* **2009**, *19*, 8772–8781.
- [9] a) Y. Zheng, A. S. Batsanov, V. Jankus, F. B. Dias, M. R. Bryce, A. P. Monkman, *J. Org. Chem.* **2011**, *76*, 8300–8310; b) P. Kautny, Z. Wu, B. Stöger, A. Tissot, E. Horkel, J. Chen, D. Ma, H. Hagemann, J. Fröhlich, D. Lumpi, *Org. Electron.* **2015**, *17*, 216–228.
- [10] a) Y. T. Tao, Q. Wang, L. Ao, C. Zhong, C. L. Yang, J. G. Qin, D. G. Ma, *J. Phys. Chem. C* **2010**, *114*, 601–609; b) Y. Tao, Q. Wang, C. Yang, C. Zhong, K. Zhang, J. Qin, D. Ma, *Adv. Funct. Mater.* **2010**, *20*, 304–311; c) P. Kautny, D. Lumpi, Y. Wang, A. Tissot, J. Binteringer, E. Horkel, B. Stöger, C. Hametner, H. Hagemann, D. Ma, J. Fröhlich, *J. Mater. Chem. C* **2014**, *2*, 2069–2081.
- [11] Z. Ge, T. Hayakawa, S. Ando, M. Ueda, T. Akiike, H. Miyamoto, T. Kajita, M.-a. Kakimoto, *Org. Lett.* **2008**, *10*, 421–424.
- [12] A. Qin, J. W. Y. Lam, B. Z. Tang, *Chem. Soc. Rev.* **2010**, *39*, 2522–2544.
- [13] a) V. V. Rostovtsev, L. G. Green, V. V. Fokin, K. B. Sharpless, *Angew. Chem. Int. Ed.* **2002**, *41*, 2596–2599; *Angew. Chem.* **2002**, *114*, 2708–2711; V. V. Rostovtsev, L. G. Green, V. V. Fokin, K. B. Sharpless, *Angew. Chem.* **2002**, *114*, 2708–2711; b) F. Amblard, J. H. Cho, R. F. Schinazi, *Chem. Rev.* **2009**, *109*, 4207–4220; c) J. E. Hein, V. V. Fokin, *Chem. Soc. Rev.* **2010**, *39*, 1302–1315; d) C. W. Tornøe, C. Christensen, M. Meldal, *J. Org. Chem.* **2002**, *67*, 3057–3064.
- [14] a) D. Lumpi, B. Stöger, C. Hametner, F. Kubel, G. Reider, H. Hagemann, A. Karpfen, J. Fröhlich, *CrystEngComm* **2011**, *13*, 7194–7197; b) D. Lumpi, F. Glöcklhofer, B. Holzer, B. Stöger, C. Hametner, G. A. Reider, J. Fröhlich, *Cryst. Growth Des.* **2014**, *14*, 1018–1031.
- [15] a) J. Li, M. Hu, S. Q. Yao, *Org. Lett.* **2009**, *11*, 3008–3011; b) S. S. Bag, R. Kundu, *J. Org. Chem.* **2011**, *76*, 3348–3356; c) A.-S. Cornec, C. Baudequin, C. Fiol-Petit, N. Plé, G. Dupas, Y. Ramondenc, *Eur. J. Org. Chem.* **2013**, 1908–1915; d) J. Shi, L. Liu, J. He, X. M. Meng, Q. X. Guo, *Chem. Lett.* **2007**, *36*, 1142–1143; e) P. D. Jarowski, Y.-L. Wu, W. B. Schweizer, F. Diederich, *Org. Lett.* **2008**, *10*, 3347–3350; f) A. Wild, C. Friebe, A. Winter, M. D. Hager, U.-W. Grummt, U. S. Schubert, *Eur. J. Org. Chem.* **2010**, 1859–1868.
- [16] M. Parent, O. Mongin, K. Kamada, C. Katan, M. Blanchard-Desce, *Chem. Commun.* **2005**, 2029–2031.
- [17] a) R. M. Meudtner, M. Ostermeier, R. Goddard, C. Limberg, S. Hecht, *Chem. Eur. J.* **2007**, *13*, 9834–9840; b) Y. H. Lau, P. J. Rutledge, M. Watkinson, M. H. Todd, *Chem. Soc. Rev.* **2011**, *40*, 2848–2866; c) J. J. Bryant, Y. Zhang, B. D. Lindner, E. A. Davey, A. L. Appleton, X. Qian, U. H. F. Bunz, *J. Org. Chem.* **2012**, *77*, 7479–7486; d) D. Schweinfurth, K. I. Hardcastle, U. H. F. Bunz, *Chem. Commun.* **2008**, 2203–2205; e) S. Ast, T. Fischer, H. Müller, W. Mickler, M. Schwichtenberg, K. Rurack, H. J. Holdt, *Chem. Eur. J.* **2013**, *19*, 2990–3005.
- [18] a) M. K. Kim, J. Kwon, T. H. Kwon, J. I. Hong, *New J. Chem.* **2010**, *34*, 1317–1322; b) M. Juriček, M. Felici, P. Contreras-Carballada, J. Lauko, S. Rodríguez-Bou, P. H. J. Kouwer, A. M. Brouwer, A. E. Rowan, *J. Mater. Chem.* **2011**, *21*, 2104–2111; c) I. Stengel, A. Mishra, N. Postrakulchote, S. J. Moon, S. M. Zakeeruddin, M. Gratzel, P. Bauerle, *J. Mater. Chem.* **2011**, *21*, 3726–3734.
- [19] Y. Zhu, S. Guang, X. Su, H. Xu, D. Xu, *Dyes Pigm.* **2013**, *97*, 175–183.
- [20] G. de Miguel, M. Wielopolski, D. I. Schuster, M. A. Fazio, O. P. Lee, C. K. Haley, A. L. Ortiz, L. Echegoyen, T. Clark, D. M. Guldi, *J. Am. Chem. Soc.* **2011**, *133*, 13036–13054.
- [21] B. Chattopadhyay, C. I. R. Vera, S. Chuprakov, V. Gevorgyan, *Org. Lett.* **2010**, *12*, 2166–2169.
- [22] Z. R. Grabowski, K. Rotkiewicz, W. Rettig, *Chem. Rev.* **2003**, *103*, 3899–4032.
- [23] N. Mataga, Y. Kaifu, M. Koizumi, *Bull. Chem. Soc. Jpn.* **1956**, *29*, 465–470.
- [24] D. A. Kleinman, *Phys. Rev.* **1962**, *126*, 1977–1979.

- [25] a) M. A. Sridhar, N. K. Lokanath, J. S. Prasad, K. S. Rangappa, N. V. Anil Kumar, D. G. Bhadre Gowda, *Mol. Cryst. Liq. Cryst. Sci. Technol. Sect. A* **1998**, 319, 137–146; b) R. Marsh, *Acta Crystallogr. Sect. A* **2004**, 60, 252–253.
- [26] D. Schweinfurth, R. Pattacini, S. Strobel, B. Sarkar, *Dalton Trans.* **2009**, 9291–9297.
- [27] C. Katan, P. Savel, B. M. Wong, T. Roisnel, V. Dorcet, J.-L. Fillaut, D. Jacquemin, *Phys. Chem. Chem. Phys.* **2014**, 16, 9064–9073.
- [28] D. Schweinfurth, S. Strobel, B. Sarkar, *Inorg. Chim. Acta* **2011**, 374, 253–260.
- [29] J. L. Oudar, D. S. Chemla, *J. Chem. Phys.* **1977**, 66, 2664–2668.
- [30] Bruker computer programs: APEX2, SAINT and SADABS (Bruker AXS Inc., Madison, WI, 2015).
- [31] L. Palatinus, G. Chapuis, *J. Appl. Crystallogr.* **2007**, 40, 786–790.
- [32] V. Petříček, M. Dušek, L. Palatinus, *Z. Kristallogr. - Cryst. Mater.* **2014**, 229, 345–352.
- [33] C. F. Macrae, P. R. Edgington, P. McCabe, E. Pidcock, G. P. Shields, R. Taylor, M. Towler, J. van de Streek, *J. Appl. Crystallogr.* **2006**, 39, 453–457.
- [34] S. K. Kurtz, T. T. Perry, *J. Appl. Phys.* **1968**, 39, 3798–3813.
- [35] A. Cwiklicki, K. Rehse, *Arch. Pharm.* **2004**, 337, 156–163.
- [36] K. D. Grimes, A. Gupte, C. C. Aldrich, *Synthesis* **2010**, 1441–1448.
- [37] F. Li, Y. Park, J. M. Hah, J. S. Ryu, *Bioorg. Med. Chem. Lett.* **2013**, 23, 1083–1086.
- [38] a) S. Ladouceur, A. M. Soliman, E. Zysman-Colman, *Synthesis* **2011**, 3604–3611; b) P. LaBeaume, K. Wager, D. Falcone, J. Li, V. Torchilin, C. Castro, C. Holewa, A. E. Kallmerten, G. B. Jones, *Bioorg. Med. Chem.* **2009**, 17, 6292–6300.
- [39] R. Anémian, D. C. Cupertino, P. R. Mackie, S. G. Yeates, *Tetrahedron Lett.* **2005**, 46, 6717–6721.
- [40] Gaussian 09, Revision D.01, M. J. Frisch, G. W. Trucks, H. B. Schlegel, G. E. Scuseria, M. A. Robb, J. R. Cheeseman, G. Scalmani, V. Barone, B. Menucci, G. A. Petersson, H. Nakatsuji, M. Caricato, X. Li, H. P. Hratchian, A. F. Izmaylov, J. Bloino, G. Zheng, J. L. Sonnenberg, M. Hada, M. Ehara, K. Toyota, R. Fukuda, J. Hasegawa, M. Ishida, T. Nakajima, Y. Honda, O. Kitao, H. Nakai, T. Vreven, J. A. Montgomery Jr., J. E. Peralta, F. Ogliaro, M. J. Bearpark, J. Heyd, E. N. Brothers, K. N. Kudin, V. N. Staroverov, R. Kobayashi, J. Normand, K. Raghavachari, A. P. Rendell, J. C. Burant, S. S. Iyengar, J. Tomasi, M. Cossi, N. Rega, N. J. Millam, M. Klene, J. E. Knox, J. B. Cross, V. Bakken, C. Adamo, J. Jaramillo, R. Gomperts, R. E. Stratmann, O. Yazyev, A. J. Austin, R. Cammi, C. Pomelli, J. W. Ochterski, R. L. Martin, K. Morokuma, V. G. Zakrzewski, G. A. Voth, P. Salvador, J. J. Dannenberg, S. Dapprich, A. D. Daniels, Ö. Farkas, J. B. Foresman, J. V. Ortiz, J. Cioslowski, D. J. Fox, Gaussian, Inc., Wallingford, CT, USA, **2009**.
- [41] a) C. Lee, W. Yang, R. G. Parr, *Phys. Rev. B* **1988**, 37, 785–789; b) A. D. Becke, *J. Chem. Phys.* **1993**, 98, 5648–5652.
- [42] R. Krishnan, J. S. Binkley, R. Seeger, J. A. Pople, *J. Chem. Phys.* **1980**, 72, 650–654.
- [43] R. Dennington, T. Keith, J. Millam, Semichem, Inc., Shawnee Mission, KS, **2009**.

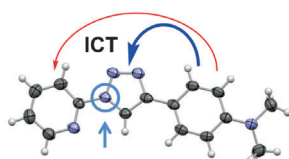
Received: July 25, 2016

Published online on ■ ■ ■■, 0000

FULL PAPER



Making connections: An in-depth analysis of the photophysical properties of a large set of 1,2,3-triazole-linked donor–acceptor materials unveiled an



intriguing relationship between the triazole substitution pattern and intramolecular charge-transfer (ICT) phenomena (see figure).

Charge Transfer

P. Kautny, D. Bader, B. Stöger,
G. A. Reider, J. Fröhlich, D. Lumpi*



**Structure–Property Relationships in
Click-Derived Donor–Triazole–
Acceptor Materials**

